Hydroxyl Radical in Aqueous Solution: Computer Simulation

Igor M. Svishchev* and Andriy Y. Plugatyr
Department of Chemistry, Trent University, Peterborough, Canada K9J 7B8
Received: August 18, 2004; In Final Form: November 18, 2004

Molecular dynamics simulations of hydroxyl radical in water are carried out by use of a classical simple point charge extended (SPC/E) water model and a similar point charge model for hydroxyl radical. Structural and dynamical properties are studied along the coexistence curve of SPC/E water at 298, 373, 473, 573, and 633 K and above its critical point at 683, 733, 783, and 833 K with density fixed at 0.3 g/cm^3. Dramatic changes in the diffusion dynamics of water and hydroxyl radical near the critical point are related to the reorganization of the three-dimensional structure of water around hydroxyl radical, as revealed by the study of the spatial distribution functions. This study helps us understand the kinetics of oxidation reactions in high-temperature water.

1. Introduction

One of the most promising industrial applications of high-temperature water is the supercritical water oxidation (SCWO) technology. Its ability to safely destroy most dangerous materials, such as PCBs, organochlorine pesticides, chemical warfare agents, etc., with high efficiency makes SCWO technology an attractive alternative to incineration and wet air oxidation methods now commonly used.

Over the last two decades significant efforts have been spent on the study of oxidation reaction kinetics in sub- and supercritical water for various chemicals[1−5] and on the determination of the optimum operating conditions for the SCWO process (pressure, temperature, type and amount of oxidizer, residence time, etc.).[6−17] At present, most SCWO applications utilize hydrogen peroxide as an oxidizing agent. H_2O_2 is an efficient oxidizer due to its rapid decomposition at high temperature to one of the most powerful oxidizing species, hydroxyl radical.[9,14] Despite significant research activity, still very little is known about the behavior of the oxidizable compounds and principal oxidizer species (such as OH) in the high-temperature aqueous medium on the molecular level. One might speculate that liquid-state reactions are diffusion-controlled and the interaction occurs at the moment when two molecules encounter each other in the solvent medium. In this case, the individual oxidation reaction rate and, ultimately, the overall degradation efficiency of the oxidation process will be related to the self-diffusion coefficients of reacting molecules. Understanding the microscopic, molecular-level picture of oxidation reactions in ambient and supercritical water is, hence, crucial for developing versatile applications of the SCWO technology.

Computer simulations have now become an important tool in the studies of liquid-state structure and dynamics. The goal of this study is to elucidate the behavior of a small dipolar molecule, hydroxyl radical, in water under normal and supercritical conditions by a computer simulation. The structural properties are studied with the aid of radial and spatial distribution functions. The average coordination number and the number of hydrogen bonds of water and of hydroxyl radical are reported. The self-diffusion coefficients of water and hydroxyl radical are also calculated and analyzed.

* Corresponding author: phone 1-705-748-1011, ext. 7063; fax 1-705-748-1625; e-mail isvishchev@trentu.ca.

The remainder of this paper is organized as follows. Computational details are described in section 2. Simulation results are discussed in section 3. Our conclusions are given in section 4.

2. Computational Details

The simple point charge extended (SPC/E) model of Berendsen et al.[18] for water was used in this study. To classically describe the OH radical, a similar point charge model for OH^- [19,20] was used, with overall charge of the molecule being set to zero. The charges, geometry, and Lennard-Jones (LJ) parameters of employed models are given in Table 1.

It is worthwhile mentioning that literature provides no rigid point charge model for OH radical that is fitted to the potential energy surface for water−OH dimer. Akiya and Savage[21] characterized the water−OH dimer interaction by using a flexible TJE model for water molecule and a flexible OH model that uses density functional theory- (DFT-) derived charges. They analyzed the structure of supercritical water−hydroxyl mixture, yet no results for fluid dynamics were provided. We have chosen to utilize the rigid point charge models for both OH and H_2O because of their simplicity in use, transferability,[19] and ability to capture the essential properties of simulated liquids. In particular, we find that our simulated self-diffusion coefficient for OH radical in water is, essentially, the same (within the statistical uncertainty) as its commonly accepted estimate from kinetic measurements[22] (2.3×10^{-9} m^2/s at 25 °C).

Simulations were carried out in the NVT ensemble along the coexistence curve of the SPC/E water at 298, 373, 473, 573, and 633 K and above the critical point at 683, 733, 783, and 833 K with density fixed at 0.3 g/cm^3. The system size was 215 water molecules and one hydroxyl radical molecule. The translational equations of motions were integrated by use of the fourth-order Gear algorithm[23] and the rotational degrees of freedom were represented by quaternions,[24] with a time step of 1 fs. Simulation run lengths are given in Table 2. The long-range Coulomb forces were evaluated by the Ewald summation technique in cubic periodic boundary conditions. The cutoff distance for the LJ interactions was set at half the cell length. The translational self-diffusion coefficients were calculated from the mean-square displacements, the statistical uncertainty being around 10% at 298 K and around 40% at 833 K.

10.1021/jp046273o CCC: $30.25
Published on Web 02/10/2005

TABLE 1: Interaction Potential Parameters, Partial Charges, and Geometries of SPC/E Water and OH Radical Models

	ϵ, kJ/mol	σ, Å	q, e	r(OH), Å	∠HOH, deg	ref
H_2O	0	0	0.4238(H)	1.000	109.47	18
	0.6517(O)	3.166(O)	−0.8476(O)			
•OH	0.231(H)	2.083(H)	0.30(H)	0.953		20
	0.632(O)	3.233(O)	−0.30(O)			

TABLE 2: MD Simulation Times

temperature, K	simulation time, ps
298	650
373	1100
473	300
573	600
633	600
683	600
733	1500
783	1600
833	1800

The simulations were carried out on a Dec-Alpha 600 workstation, Department of Chemistry, Trent University.

3. Results and Discussion

(a) Radial Distribution Function. Changes in water structure with temperature have been previously analyzed in a number of experimental and simulation studies (see refs 25−27 and references therein). In this work we will focus on the hydration of a small dipolar molecule, hydroxyl radical, as seen by a computer simulation.

The oxygen (H_2O)−oxygen (OH), oxygen (H_2O)−hydrogen (OH), and hydrogen (H_2O)−oxygen (OH) radial distribution functions (RDFs) are displayed in Figure 1. The coordination number, n_{OO}, for water around water and for water around OH, together with the number of hydrogen bonds, n_{HB}, that water and hydroxyl radical form, are given in Figure 2. The coordination number is determined from the integration of the first maximum of the corresponding oxygen−oxygen RDF (of water−water or water−hydroxyl distributions), while the number of hydrogen bonds is determined from the integration of the first maximum of the corresponding oxygen−hydrogen RDFs.[27] At ambient temperature the first coordination shell of hydroxyl radical is represented by a broad peak in oxygen (H_2O)−oxygen (OH) RDF centered at 3.25 Å (with minimum at 5 Å), as can be seen in Figure 1a. As one might expect, the second peak is hardly discernible, which indicates that there is little tendency for specific ordering of water molecules beyond the first hydration sphere around OH. It is worth mentioning that the maxima of oxygen (H_2O)−oxygen (OH) RDF correspond to the local minima between the first and second hydration shells of O (H_2O)−O (H_2O) RDF; see Figure 3a. This suggests that hydroxyl radical tends to occupy "cavities" in the H-bond network of water. Coordination number for water molecules around OH, n_{OO}, obtained from the integration of the first peak of $g_{OO}(R)$ was found to be approximately 16 at 298 K, which indicates a quasi-clathrate structure formed by water molecules around a hydroxyl radical molecule.

Intuitively, one might expect that hydroxyl radical participates in H-bonding in liquid water similar to any water molecule, by forming both donor and acceptor H-bond pairs. Surprisingly, a single broad peak centered at a rather large separation of 3.25 Å in hydrogen (H_2O)−oxygen (OH) RDF gives no indication of an H-bond-like arrangement. However, examination of oxygen (H_2O)−hydrogen (OH) RDF shows two peaks, one at 2 Å and another at 4 Å. The position of this first peak is very close to the position of the first peak of oxygen−hydrogen RDF of water itself, at 1.8 Å, and falls within the range of the geometrical condition for the presence of hydrogen bond[27] (r < 2.4 Å). Integration of this first peak indicates the presence of one H-bonded-like complex of OH with water molecule, namely, n_{HB} = 1.05. Therefore, hydroxyl radical acts only as an H-bond donor (no tendency for accepting H-bonds).

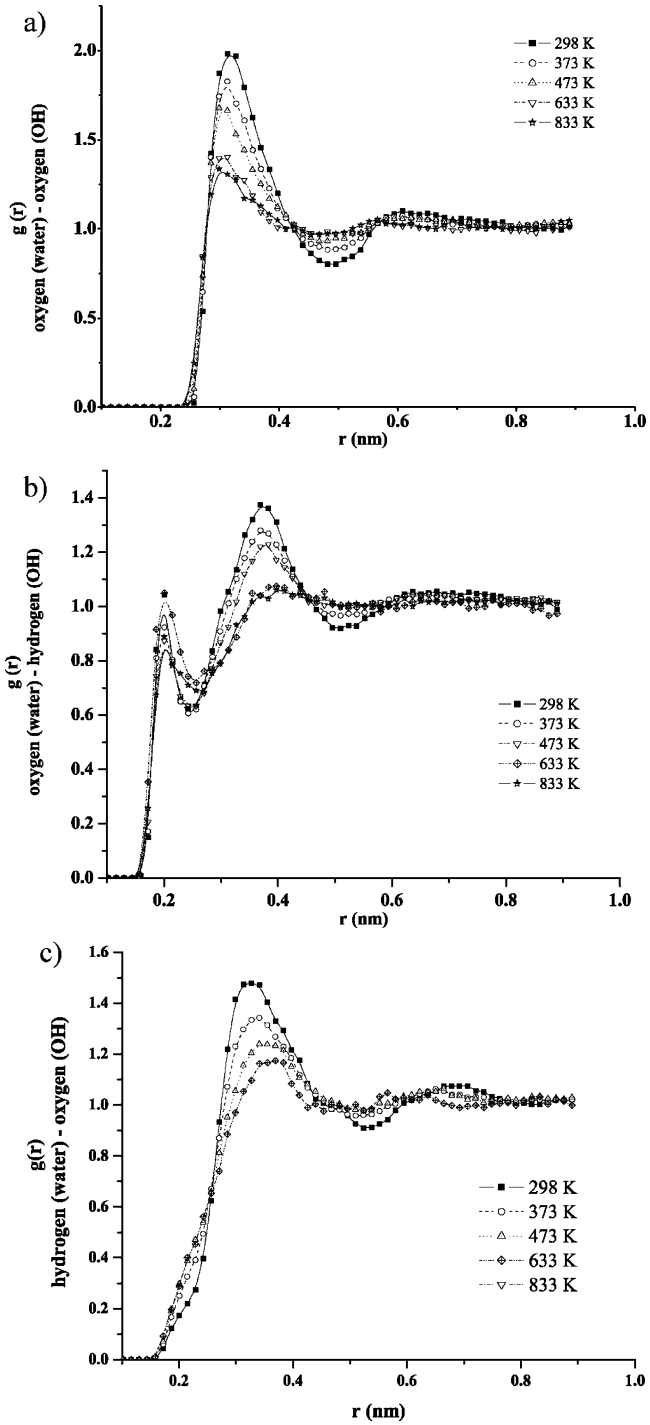

Figure 1. Radial distribution function for (a) oxygen (H_2O)−oxygen (OH), (b) oxygen (H_2O)−hydrogen (OH), and (c) hydrogen (H_2O)−oxygen (OH) pairs.

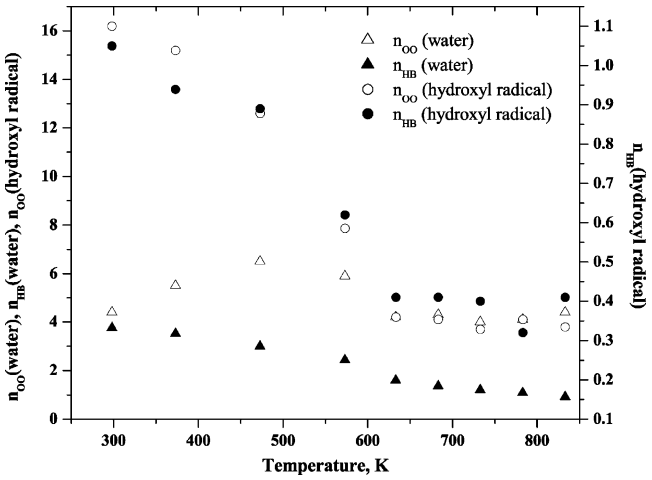

Figure 2. Coordination number, n_{OO}, and number of hydrogen bonds, n_{HB}, for water and hydroxyl radical.

As temperature increases toward the critical point, the network of H-bonds in liquid water undergoes significant changes. As can be seen in Figure 3b−e, the peaks of the first and second H-bonded neighbors in water−water RDF $g_{OO}(R)$ shift from 2.75 and 4.5 Å at room temperature to 3 and 5.5 Å at the critical point (T_c is around 633 K for the SPC/E water), respectively. At the same time, higher temperature allows for non-hydrogen-bonded molecules to enter the first coordination sphere of water. As a result, the coordination number of water around water increases to approximately 6 at 473 K. It then decreases to 4 at 633 K, as the effect of decreasing density in near-critical water prevails. Similar observations were reported by Guissani and Guillot.[27] The number of hydrogen bonds per water molecule gradually decreases from 3.8 at 298 K, the number that reflects tetrahedral coordination of nearest neighbors, to 1.6 at 633 K (near the critical point) and to about 1 at 833 K (in supercritical fluid).

Remarkable changes in liquid structure are also well-illustrated by the temperature evolution of the oxygen (H_2O)−oxygen (OH) RDF. As temperature increases, the first peak in this RDF shifts from 3.25 to 3 Å (in contrast with the water−water RDF, where it shifts from 2.8 to 3 Å), which indicates that hydroxyl radical has a much higher tendency for entering the first coordination shell of water at higher temperatures. The second peak in the water−hydroxyl radical RDFs disappears around 473 K, as can be seen in Figure 3c, indicating disappearance of interparticle correlations beyond the first hydration sphere of OH. Above the critical point, hydroxyl radical virtually behaves like another water molecule; the positions of the first peaks in oxygen (H_2O)−oxygen (H_2O) and oxygen (H_2O)−oxygen (OH) RDFs are virtually the same (unlike those at low temperatures). This observation is confirmed by the calculation of the average number of water molecules around hydroxyl radical. It approximately equals 4 above the critical point (same number as for water). The average number of H-bond complexes in which OH formally[27] participates within its first coordination sphere decreases from about 1 at 298 K (one donor H-bond with water molecule) to about 0.4 at supercritical conditions.

(b) Spatial Distribution Function. Structure in molecular liquids can only be fully characterized by the spatial distribution function (SDF).[28] SDF, $g(r, \Omega)$, in contrast with RDF, $g(r)$, accounts for both radial, r, and angular, Ω, atom−atom correlations, allowing for the construction of the three-dimensional (3D) visualization of local atomic densities.

In this work, we use SDF to study solvation structure of hydroxyl radical−water mixture. SDF is normally presented by use of isodensity surfaces at some probability level, for instance, higher than that of the bulk system. Figure 4a represents average local 3D structure of water at 298 K. Dark gray areas represent the SDFs of oxygen atoms of water molecules around a central water molecule at $g(r, \Omega) = 1.85$. Spatial hydration structures of water have been explicitly described previously.[25] Here we provide only a concise interpretation of water−water SDF in order to guide the reader through the remainder of the paper. In Figure 4a the oxygen atoms in the SDF of water molecule are represented by five distinct features. Two caps positioned in the direction of OH bond are due its two H-bond-accepting neighbors, one large cupped feature below the central molecule is due to its two H-bond-donating neighbors, and two more distant features are due to the additional nontetrahedral coordination. At high temperatures, as thermal motion of molecules increases, the average spatial distributions of atoms gets wider; hence, the larger areas are covered by surfaces in Figure 4b,c. Also, the features due to nontetrahedral coordination and H-bond-donating neighbors merge into a single wide feature spanning a large surface area located mainly in the lower part of the principal frame of the central molecule, which can be clearly seen in Figure 4c.

Figure 5 illustrates spatial orientation of oxygen atoms (gray areas) and hydrogen atoms (light gray areas) of hydroxyl radical around water molecule at $g(r, \Omega) = 2$ at 298 K. A notable feature in this spatial map is that the pair-density distributions, due to OH radical, occupy those regions of the space that are not occupied by the tetrahedral pair-density features of water's oxygen atoms, those that are shown in Figure 4a. This figure clearly proves that OH radical tends to occupy the nontetrahedral positions around water molecule ("holes" in water structure) at room temperature. Close examination of the hydrogen (OH)−oxygen (H_2O) SDF also shows that OH radical is capable of entering the first coordination sphere of water only as H-bond donor, as indicated by a cupped feature below the central oxygen atom of water. Despite the tetrahedral orientations of more distant positions of oxygen atoms of hydroxyl radical along the OH bond axis of the central water molecule (Figure 5a), their positions are at very large separations (of about 3.8 Å) and cannot be viewed as an indication of an H-bond acceptor.

As temperature increases, the average structure of water around OH becomes less pronounced, which can be seen in Figure 6; all peaks undergo significant broadening. The temperature also has an effect on the relative orientation of OH with respect to water molecules. Spatial positions of O atoms in OH radical with respect to coordinated water molecule become very similar to spatial positions of O atoms in water molecules around water at 633 K. This indicates that while at low temperatures OH behaves as a largely distinct species with a preference for formation of a quasi-clathrate cage, at higher (near and supercritical) temperatures it becomes virtually indistinguishable, from a structural viewpoint, from surrounding water molecules.

(c) Self-Diffusion Coefficient. The self-diffusion coefficients of water and hydroxyl radical were calculated in order to examine the dynamical properties of the simulated system. Our results, along with previously published experimental and theoretical data,[27,29−31] are given in Figure 7.

As expected, the self-diffusion coefficients of water and OH radical increase with temperature. Kinetic mobility of water and the OH radical rises dramatically near the critical region. A particularly interesting observation concerns the behavior of the

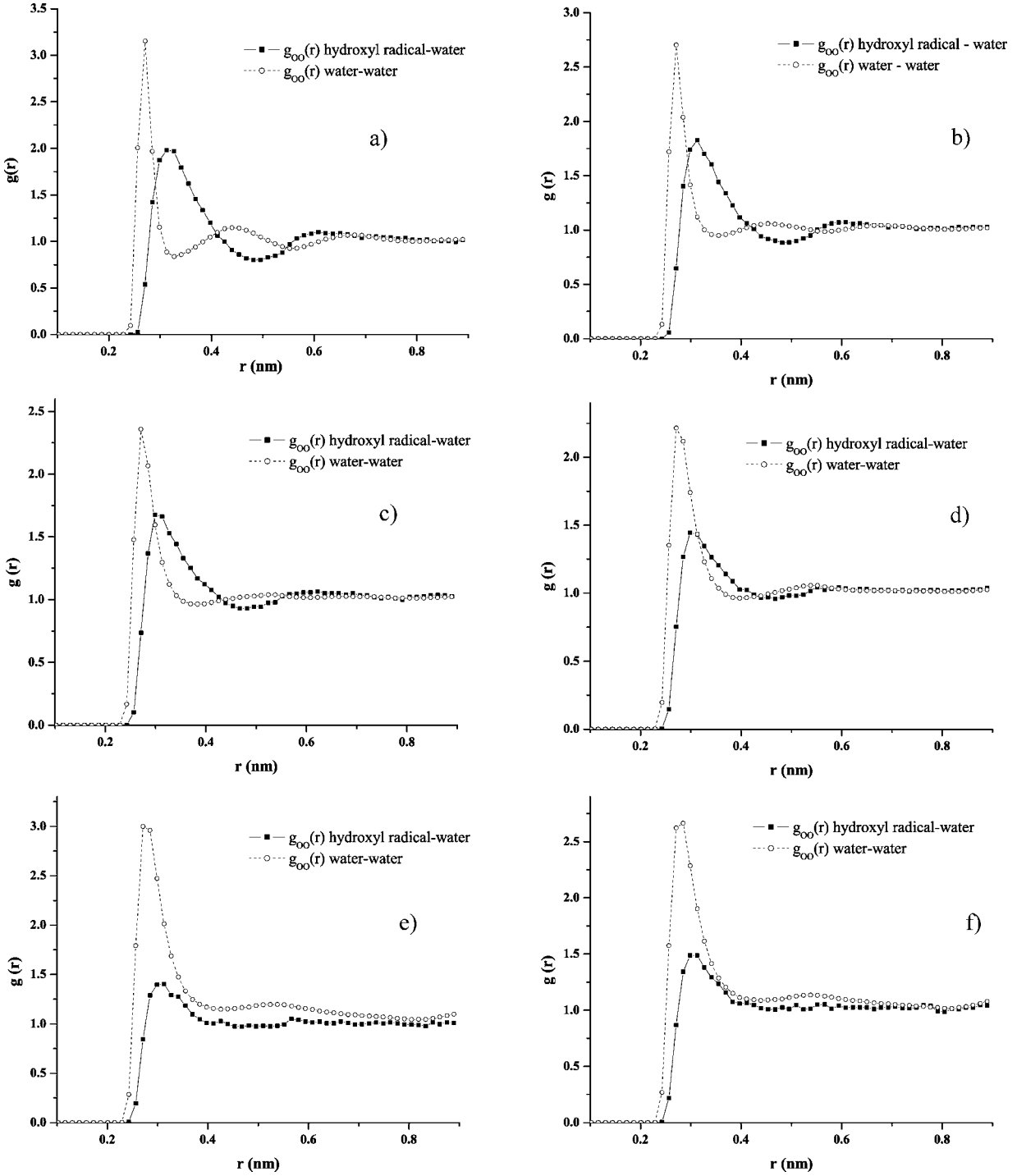

Figure 3. Radial distribution function for oxygen−oxygen (H_2O) and oxygen (OH radical)−oxygen (H_2O) pairs at (a) 298, (b) 373, (c) 473, (d) 573, (e) 633, and (f) 683 K.

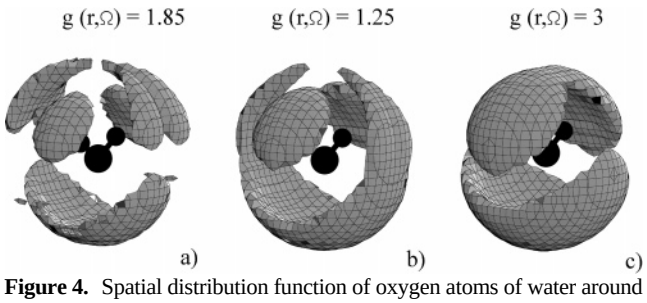

Figure 4. Spatial distribution function of oxygen atoms of water around central water molecule at (a) 298, (b) 473, and (c) 633 K.

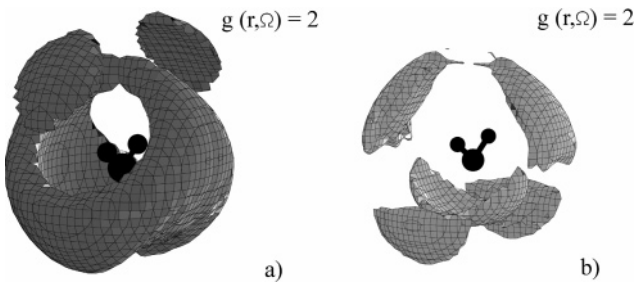

Figure 5. Spatial distribution function of (a) oxygen and (b) hydrogen atoms of hydroxyl radical around central water molecule at 298 K.

hydroxyl radical species. The self-diffusion coefficient of OH is smaller than that of water below the critical point, despite its lower mass. Thus, one might conclude that the diffusion of OH radical in water under ambient conditions (in high-density

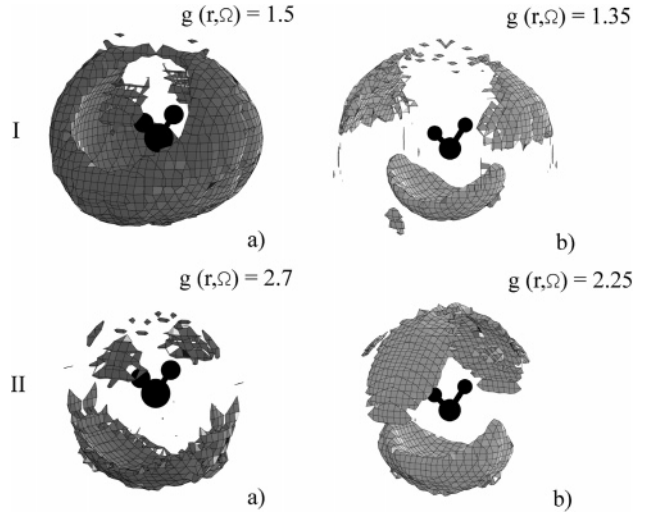

Figure 6. Spatial distribution function of (a) oxygen and (b) hydrogen atoms of hydroxyl radical around central water molecule at (I) 473 and (II) 633 K.

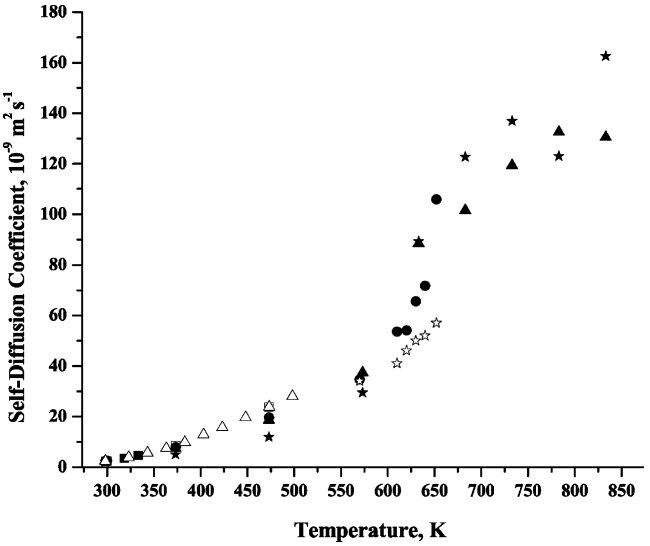

Figure 7. Self-diffusion coefficient of water and hydroxyl radical. (△) H_2O, exptl[29]; (□) H_2O, exptl[30]; (☆) H_2O, exptl[31]; (●) H_2O, simulation[27]; (▲) H_2O, simulation (this study); (★) OH radical, simulation (this study).

solvent) is hindered by the H-bond network of water structure. In other words, below the critical point OH does not diffuse as "another" water molecule but rather acts as a "foreign" species forming a quasi-clathrate hydrate structure. This observation is fully consistent with the analysis of the atom−atom radial and spatial distribution functions in sections 3a and 3b. In contrast, the dynamics of OH molecules are faster than that of water above the critical point. Under these conditions water behaves as a low-polarity solvent that does not form the three-dimensional H-bond network. Apparently the OH radical, because of its lesser ability to form hydrogen bonds with water molecules, has more freedom to move in the absence of the three-dimensional network of hydrogen bonds that hinders its diffusion in the ambient liquid.

The behavior of the self-diffusion coefficients of water and OH radical below, near, and above the critical point of water is strikingly reminiscent of the behavior of the degradation efficiency of oxidation reactions involving OH.[32] It has been found that the oxidation of hydrophobic organic compounds becomes particularly fast near the critical point. Furthermore, it has been argued that the corrosion activity of the oxygenated aqueous medium (in which OH also plays a key role) also exhibits a dramatic rise near the critical point followed by a much lesser increase with temperature under supercritical conditions.[33,34] Our MD simulation results seem to provide some theoretical support for these experimental observations. We argue that the unique microdynamic properties of dissolved species (high diffusivity of principal oxidant OH and its unique solvation at high temperatures) largely explain the elevated efficiency of aqueous oxidation reactions near and above the critical point, making the SCWO degradation process very rapid and complete. Clearly, further investigations of the relationship between microdynamic properties of SCW and its oxidation ability are warranted.

4. Conclusion

We have examined the structure and dynamics in hydroxyl radical−water mixture along the coexistence curve for SPC/E water and in supercritical states with the density fixed at 0.3 g/cm^3, as in typical SCWO experiments.

Careful inspection of the spatial liquid structures indicates that below the critical point of water OH radical occupies "holes" in tetrahedral arrangements of water molecules. Above the critical point OH radical behaves like another water molecule.

Self-diffusion coefficients of water and the OH molecular radical were calculated. The temperature variation of the self-diffusion coefficients of water and OH radical below, near, and above the critical point of water is similar to the variation of the degradation efficiency of oxidation reactions. We speculate that the high mobility of the key oxidizing species, OH, in supercritical water together with the change in its hydration is one of the key factors responsible for the high degradation potency of the SCWO process.

Acknowledgment. This work was done with the financial support of the Natural Sciences and Engineering Council of Canada.

References and Notes

(1) Savage, P. E.; Yu, J.; Stylski, N.; Brock, E. E. *J. Supercrit. Fluids* **1998**, *12*, 141.
(2) Brock, E. E.; Savage, P. E.; Barker, J. R. *Chem. Eng. Sci.* **1998**, *53*, 857.
(3) Rice, S. F.; Steeper, R. R. *Hazard. Mater. J.* **1998**, *59*, 261.
(4) Gopalan, S.; Savage, P. E. *AIChE J.* **1995**, *41*, 1864.
(5) Martino, C. J.; Savage, P. E. *Ind. Eng. Chem. Res.* **1997**, *36*, 1391.
(6) Goto, M.; Nada, T.; Ogata, A.; Kodama, A.; Hirose, T. *J. Supercrit. Fluids* **1998**, *13*, 277.
(7) Ahn, S. H.; Joung, S. N.; Yoo, K.-P.; Noh, M. J.; Han, J. H.; Han, S. H. *Korean J. Chem. Eng.* **1998**, *15*, 390.
(8) Anitescu, G.; Tavlarides, L. L. *Ind. Eng. Chem. Res.* **2000**, *39*, 583.
(9) Lee, D.-S.; Gloyna, E. F.; Li, L. *J. Supercrit. Fluids* **1990**, *3*, 249.
(10) Hatakeda, K.; Ikushima, Y.; Sato, O.; Aizawa, T.; Saito, N. *Chem. Eng. Sci.* **1999**, *54*, 3079.
(11) Kanthasamy, A.; Gloyna, E. F. Technical Report CRWR 242; University of Texas at Austin: Austin, TX, 1994.
(12) Blanks, M. E.; Gloyna, E. F. Technical Report CRWR 238; University of Texas at Austin: Austin, TX, 1992.
(13) Crain, N. E.; Gloyna, E. F. Technical Report CRWR 241; University of Texas at Austin: Austin, TX, 1993.
(14) Croiset, E.; Rice, S. F.; Hanush, R. G. *AIChE J.* **1997**, *43*, 2343.
(15) Lin, K.-S.; Wang, H. P. *Environ. Sci. Technol.* **1999**, *33*, 3278.
(16) Weber, R.; Yoshida, S.; Miwa, K. *Environ. Sci. Technol.* **2002**, *36*, 1839.
(17) Matsumara, Y.; Nunoura, T.; Urase, T.; Yamamoto, K. *J. Hazard. Mater.* **2000**, *B73*, 245.
(18) Berendsen, H. J. C.; Grigera, J. R.; Straatsma, T. P. *J. Phys. Chem.* **1987**, *91*, 6269.
(19) Weiner, S. J.; Kollman, P. A.; Nguyen, D. T.; Case, D. A. *J. Comput. Chem.* **1986**, *7*, 230.

(20) Balbuena, P. B.; Johnston, K. P.; Rossky, P. J. *J. Phys. Chem.* **1996**, *100*, 2706.
(21) Akiya, N.; Savage, P. E. *J. Phys. Chem. A* **2000**, *104*, 4433.
(22) Baxton, G. V.; Greenstock, C. L.; Helman, W. P.; Ross, A. B. *J. Phys. Chem. Ref. Data* **1988**, *17*, 513.
(23) Evans, D. J.; Morriss, J. P. *Comput. Phys. Rep*. **1984**, *1*, 297.
(24) Evans, D. J. *Mol. Phys*. **1977**, *34*, 317.
(25) Svishchev, I. M.; Zassetsky, A. Yu.; Kusalik, P. G. *Chem. Phys*. **2000**, *258*, 181.
(26) Jedlovszky, P.; Brodholt, J. P.; Bruni, F.; Ricci, M. A.; Soper, A. K.; Vallauri, R. *J. Chem. Phys*. **1998**, *108*, 8528.
(27) Guissani, Y.; Guillot, B. *J. Chem. Phys*. **1993**, *98*, 8221.
(28) Kusalik, P. G.; Svishchev, I. M. *Science* **1994**, *265*, 1219.
(29) Krynicki, K.; Green, C. D.; Sawyer, D. W. *Faraday Discuss. Chem. Soc.* **1980**, *66*, 199.
(30) Harris, K. R.; Woolf, L. A. *J. Chem. Soc., Faraday Trans*. **1980**, *76*, 377.
(31) Hausser, R.; Maier, G.; Noack, F. *Z. Naturforsch.* **1966**, *21a*, 1410.
(32) Svishchev, I. M.; Plugatyr, A. Y.; Hayward, T. M. *J. Supercrit. Fluids* (submitted for publication).
(33) Kritzer, P.; Boukis, N.; Dinjus, E. *J. Supercrit. Fluids* **1999**, *15*, 205.
(34) Hayward, T. M.; Svishchev, I. M.; Makhija, R. C. *J. Supercrit. Fluids* **2003**, *27*, 275.